

# The anomalous $Zb\bar{b}$ couplings: From LEP to LHC

Bin Yan<sup>1,\*</sup> and C.-P. Yuan<sup>2,†</sup>

<sup>1</sup>Theoretical Division, Group T-2, MS B283, Los Alamos National Laboratory, P.O. Box 1663, Los Alamos, NM 87545, USA

<sup>2</sup>Department of Physics and Astronomy, Michigan State University, East Lansing, MI 48824, USA

The bottom quark forward-backward asymmetry ( $A_{FB}^b$ ) data at LEP exhibits a long-standing discrepancy with the standard model prediction. We propose a novel method to probe the  $Zb\bar{b}$  interactions through  $gg \rightarrow Zh$  production at the LHC, which is sensitive to the axial-vector component of the  $Zb\bar{b}$  couplings. We demonstrate that the  $Zh$  data collected at the 13 TeV LHC can already resolve the apparent degeneracy of the anomalous  $Zb\bar{b}$  couplings implied by the LEP precision electroweak measurements, with a strong dependence on the observed distribution of the  $Z$  boson transverse momentum. We also show the potential of the HL-LHC to either verify or exclude the anomalous  $Zb\bar{b}$  couplings observed at LEP through measuring the  $Zh$  production rate at the HL-LHC, and this conclusion is not sensitive to possible new physics contribution induced by top quark or Higgs boson anomalous couplings in the loop.

**Introduction:** The LEP and SLC experiments have measured the  $Z$  boson couplings and found most of the electroweak data are consistent with the standard model (SM) predictions with a remarkable precision [1]. However, there are still some experimental results which cannot be explained within the SM framework. A notorious example is that the bottom quark forward-backward asymmetry ( $A_{FB}^b$ ) measured at the LEP presents a  $2.5\sigma$  deviation with respect to the SM prediction [1]. As a result, it requires some degree of tuning of the left and right-handed  $Zb\bar{b}$  couplings. One class of intriguing models proposed in the literature to explain the puzzling  $A_{FB}^b$  data is to allow a sizable right-handed  $Zb\bar{b}$  coupling, while keeping the left-handed  $Zb\bar{b}$  coupling about the same as the SM value [2–4]. Although such a large discrepancy in  $A_{FB}^b$  could be an evidence of new physics (NP) beyond the SM, it is also important to exclude the possibility that it was caused by statistical fluctuation or some subtle systematic errors in experiments. Resolving this puzzle has become one of the core tasks of the next generation lepton colliders, e.g. CEPC, ILC, CLIC and FCC-ee, which has received much attention by the high energy physics community [5–8]. However, a direct measurement of the  $Zb\bar{b}$  couplings at the Large Hadron Collider (LHC) is often ignored in the literature due to the huge backgrounds for detecting the  $Z$  boson decaying into a bottom quark and antiquark pair, *i.e.*,  $Z \rightarrow b\bar{b}$ .

In this Letter, we propose a novel method to probe the  $Zb\bar{b}$  couplings through the associated production of  $Z$  and Higgs boson ( $h$ ) via  $gg \rightarrow Zh$  at the LHC. The  $Zb\bar{b}$  couplings contribute to the  $Zh$  associated production through bottom quark loop effects in gluon fusion channel, cf. Fig. 1. This process has been widely used to constrain the top quark anomalous couplings, e.g.  $Zt\bar{t}$ ,  $ht\bar{t}$ , and it has been shown to be sensitive to many NP effects [9–18]. For the first time, we demonstrate that this process can also be used to constrain the bottom quark anomalous couplings and to resolve the  $A_{FB}^b$  puzzle.

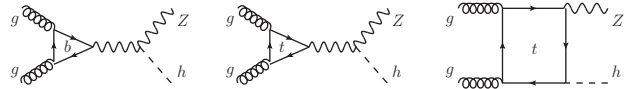


FIG. 1. Illustrative Feynman diagrams of  $gg \rightarrow Zh$  production at the LHC.

Owing to charge conjugation invariance, the  $Z$ -boson couples only axially to the internal quarks in the loop of diagrams shown in Fig. 1, so that the contribution from a mass-degenerate weak doublet of quarks vanishes. Such property leads to the conclusion that the  $gg \rightarrow Zh$  production in the SM would only be sensitive to physics of the third generation quarks, *i.e.*, the bottom and top quarks. Furthermore, as to be shown below, the contribution from the bottom quark is comparable to the top quark in  $gg \rightarrow Zh$  production. Therefore, such process could be used to probe the axial-vector component of the  $Zb\bar{b}$  interaction at hadron colliders.

The main difficulty of measuring the  $Zb\bar{b}$  couplings at the LHC via  $gg \rightarrow Zh$  process comes from the contamination of the top quark contribution in the loop. It is well known that there is a top quark threshold effect when the invariant mass ( $m_{Zh}$ ) of  $Z$  and  $h$  larger than about twice of top quark mass ( $m_t$ ), which is related to the absorptive part of gluon-gluon fusion amplitude for producing an on-shell  $t\bar{t}$  pairs. Therefore, any new physics related to top quark could be tested through the invariant mass distribution near the top quark threshold. One can also combine the other measurements at the LHC to constrain the top quark anomalous couplings, e.g.  $Zt\bar{t}$  and  $ht\bar{t}$  couplings [19–24]. In this letter, we demonstrate that one could determine the  $Zb\bar{b}$  couplings through detecting  $Zh$  associated production at the LHC, and the results are not sensitive to the top quark nor the Higgs boson anomalous couplings. Furthermore, we show that the implication of the  $A_{FB}^b$  data at LEP can either be verified or excluded if the central value of the signal strength is found to be less

than what SM predicts at the High luminosity LHC (HL-LHC), a proton-proton collider to operate at a center-of-mass energy of 14 TeV with an integrated luminosity of  $3 \text{ ab}^{-1}$ . In that case, our method can also resolve the degeneracy of the  $Zb\bar{b}$  couplings, presently allowed by the precision electroweak data at LEP and SLC.

**$Zh$  production via gluon fusion:** We consider the following effective Lagrangian related to  $Zh$  associated production,

$$\begin{aligned} \mathcal{L} = & \frac{g_W}{2c_W} \bar{b} \gamma_\mu (\kappa_v^b v_b^{\text{SM}} - \kappa_a^b a_b^{\text{SM}} \gamma_5) b Z_\mu + \frac{m_Z^2}{v} \kappa_Z h Z_\mu Z^\mu \\ & + \frac{g_W}{2c_W} \bar{t} \gamma_\mu (\kappa_v^t v_t^{\text{SM}} - \kappa_a^t a_t^{\text{SM}} \gamma_5) t Z_\mu - \frac{m_t}{v} \kappa_t \bar{t} t h, \end{aligned} \quad (1)$$

where  $g_W$  is the weak gauge coupling,  $c_W$  is the cosine of the weak mixing angle  $\theta_W$  and  $v = 246 \text{ GeV}$  is the Higgs vacuum expectation value. The gauge coupling strength modifiers  $\kappa_{v,a}^{b,t}$  and  $\kappa_{t,Z}$  are introduced to include the possible NP effects and they can be matched to the dimension-6 operators after the electroweak symmetry breaking under the SM effective field theory [25–27]. The vector and axial-vector couplings of  $Z$  boson to bottom (b) and top (t) quarks in the SM are:

$$\begin{aligned} v_b^{\text{SM}} &= -\frac{1}{2} + \frac{2}{3} s_W^2, & a_b^{\text{SM}} &= -\frac{1}{2}, \\ v_t^{\text{SM}} &= \frac{1}{2} - \frac{4}{3} s_W^2, & a_t^{\text{SM}} &= \frac{1}{2}. \end{aligned} \quad (2)$$

Here  $s_W \equiv \sin \theta_W$ . We calculate the helicity amplitudes  $M_{\lambda_1, \lambda_2, \lambda_3}$  of the channel  $g(\lambda_1)g(\lambda_2) \rightarrow Z(\lambda_3)h$  using FeynArts [28] and FeynCalc [29], where  $\lambda_i = +, -, 0$  labels the helicity of particle  $i$ . Below, we show the explicit expression of the dominant helicity amplitudes, which can be written, separately for triangle ( $\triangle$ ) and box ( $\square$ ) diagrams, as

$$\begin{aligned} M_{++0}^\triangle &= 2 \frac{\sqrt{\lambda}}{m_Z} \sum_{t,b} \left[ \kappa_a^q \kappa_Z \frac{a_q^{\text{SM}} g_{hZZ}}{m_Z^2} (F_\triangle(s, m_q^2) + 2) \right] N, \\ M_{++0}^\square &= -\frac{4}{m_Z \sqrt{\lambda}} \kappa_a^t \kappa_t g_{htt} a_t^{\text{SM}} m_t [F_{++}^0 + (t \leftrightarrow u)] N, \end{aligned} \quad (3)$$

where

$$\lambda = s^2 + m_Z^4 + m_h^4 - 2(sm_Z^2 + m_Z^2 m_h^2 + m_h^2 s), \quad N = \frac{\alpha_s g_W}{32\pi c_W}, \quad (4)$$

and  $s, t, u$  are the usual Mandelstam variables for describing the scattering of  $gg \rightarrow Zh$ . The other couplings are defined as  $g_{hZZ} = 2m_Z^2/v$  and  $g_{htt} = -m_t/v$ . The helicity amplitudes  $M_{--0}^\triangle, \square = -M_{++0}^\triangle, \square$ , while the other helicity configurations could be ignored due to their small numerical contributions, about 0.1% at the 14 TeV LHC, to the inclusive production cross section. (Although in the following numerical results, we have included contributions

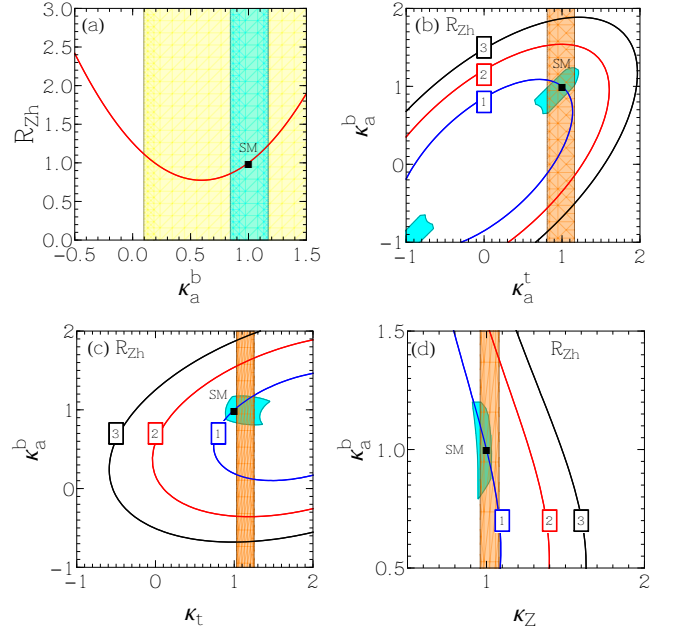


FIG. 2. The contours of  $R_{Zh}$  in the plane of anomalous couplings at the 14 TeV LHC. The cyan region denotes the constraints, at  $1\sigma$  level, provided by the measurements of  $pp \rightarrow Zh$  at the 13 TeV LHC, while the yellow shaded region denotes the impact after removing the two high  $p_T^Z$  data depicted in Fig. 4 of Ref. [32]. The orange bands in (b), (c) and (d) come from the constraints of  $Zt\bar{t}$ ,  $ht\bar{t}$  and  $hZZ$  coupling measurements at the 13 TeV LHC, respectively.

from all helicity configurations.) The definition of the scalar functions  $F_\triangle$  and  $F_{++}^0$  in Eq. (3) could be found in Ref. [30]. We have compared our analytical results to MadGraph5 [31] and found perfect agreement.

**Sensitivity at the LHC:** Below, we consider the impact of the non-standard  $Zb\bar{b}$ ,  $Zt\bar{t}$ ,  $ht\bar{t}$  and  $hZZ$  couplings to the inclusive cross section of  $gg \rightarrow Zh$  at the 14 TeV LHC. In order to compare  $\sigma(gg \rightarrow Zh)$  with the SM prediction, we define a ratio  $R_{Zh}$  as,

$$R_{Zh} = \frac{\sigma(gg \rightarrow Zh)}{\sigma(gg \rightarrow Zh)^{\text{SM}}}. \quad (5)$$

Figure 2 displays the contours of  $R_{Zh}$  in the plane of anomalous couplings. The cyan region denotes the constraints from the measurements of inclusive cross section and transverse momentum distribution of  $Z$  boson ( $p_T^Z$ ) in the  $pp \rightarrow Zh$  production at the 13 TeV LHC [32–36]. The dominant constraint on the parameter space comes from the ATLAS  $Zh$  data with high  $p_T^Z$  [32], which shows a large deviation from the central value of the signal strength ( $\mu_{Zh} \equiv \sigma(pp \rightarrow Zh)/\sigma(pp \rightarrow Zh)^{\text{SM}}$ ) predicted by the SM, i.e.  $\mu_{Zh} = 0.34_{-0.7}^{+0.75}$  and  $\mu_{Zh} = 0.28_{-0.83}^{+0.97}$  for  $p_T^Z \in [250, 400] \text{ GeV}$  and  $p_T^Z > 400 \text{ GeV}$ , respectively, cf. Fig.4 of Ref. [32]. If we exclude those two high  $p_T^Z$  data points, whose central values happen to be

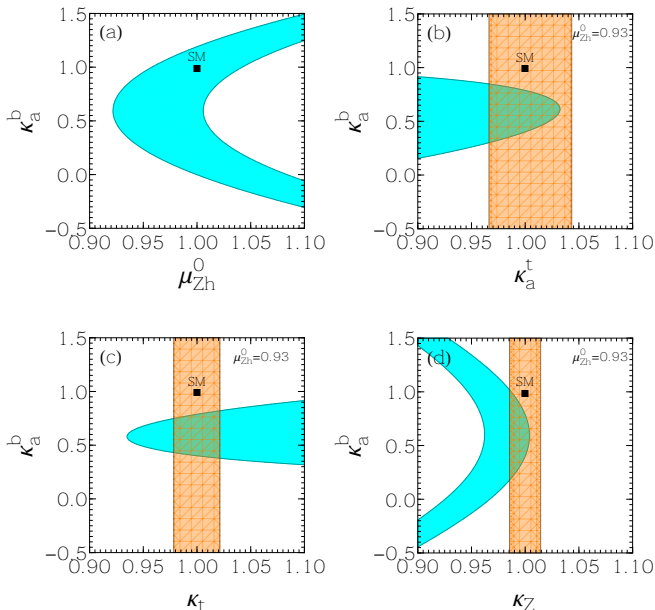


FIG. 3. Expected uncertainty for measuring the axial-vector  $Zb\bar{b}$  coupling  $\kappa_a^b$  via  $Zh$  associated production at the HL-LHC. The central value of signal strength of subfigures (b)-(d) is assumed to be  $\mu_{Zh}^0 = 0.93$ . The orange bands in (b)-(d) represent the  $1\sigma$  constraint from the  $Zt\bar{t}$ ,  $ht\bar{t}$  and  $hZZ$  coupling measurements at the HL-LHC, respectively.

much smaller than the SM predictions, the allowed parameter space is depicted as the yellow band in Fig. 2(a), which shows a much wider uncertainty in  $\kappa_a^b$  as compared to the cyan band (with  $0.84 < \kappa_a^b < 1.17$  at  $1\sigma$  level). Hence, it is important to improve the measurement of the  $p_T^Z$  distribution of  $Zh$  production at the HL-LHC. The higher order QCD correction effects are taken into account by introducing a constant  $k$ -factor for both  $q\bar{q} \rightarrow Zh$  and  $gg \rightarrow Zh$  production processes in the analysis, with  $k_{q\bar{q}} = 1.3$  and  $k_{gg} = 2.7$  [37, 38]. The orange bands in Fig. 2(b)-(d) show the constraints imposed by the measurements of  $Zt\bar{t}$ ,  $ht\bar{t}$  and  $hZZ$  couplings at the 13 TeV LHC [39–45], respectively. They were obtained by analyzing the production of  $Zt\bar{t}$ ,  $Ztj$ ,  $ht\bar{t}$  and  $gg \rightarrow h \rightarrow ZZ^*$ , etc. The cyan region shown in Fig. 2(b) is constrained by the 13 TeV  $Zh$  data while letting both  $\kappa_a^t$  and  $\kappa_v^t$  freely vary within the allowed range imposed by the measurement of  $Zt\bar{t}$  couplings. This yields only a slightly larger uncertainty band as  $0.66 < \kappa_a^b < 1.23$ . Similar analyses, but separately for the anomalous couplings  $\kappa_t$  and  $\kappa_Z$ , are shown in Fig. 2(c) and (d). Within the constraints from the current data, the cross section  $\sigma(gg \rightarrow Zh)$  could differ from the SM prediction by about 20%  $\sim$  30% (or 100%, if without the inclusion of two above-mentioned high  $p_T^Z$  data points) which is a large enough deviation that can be detected at the HL-LHC [46].

At the HL-LHC, many experimental measurements can be further improved as compared to the present data. The error of the signal strengths of  $Zh$  and  $ht\bar{t}$  productions can be reduced to about 4.2% and 4.3%, respectively, while the uncertainty of the branching ratio of  $h \rightarrow ZZ^*$  would be at 2.9% [46]. The limit on  $\kappa_a^t$  will also be highly improved through measuring the  $t\bar{t}h$ ,  $thj$  and  $gg \rightarrow ZZ$  productions [14, 24]. We summarize the expected constraints from the above production processes at the HL-LHC in Fig. 3. It shows that the expected accuracy for measuring  $\kappa_a^b$  at the HL-LHC is sensitive to the central value of the signal strength  $\mu_{Zh}^0$ , cf. Fig. 3(a). We choose two benchmark values of  $\mu_{Zh}^0$  for illustration;  $\mu_{Zh}^0 = 0.93$  (in Fig. 3) and  $\mu_{Zh}^0 = 1$  (in Fig. 4). The blue band represents the  $1\sigma$  uncertainty of the  $\kappa_a^b$  measurement, which is derived from the  $Zh$  associated production cross section. The orange shaded regions show the allowed parameter space of the  $Zt\bar{t}$ ,  $ht\bar{t}$  and  $hZZ$  coupling measurements at the HL-LHC when we consider only two parameters at a same time [46]. It shows that  $\kappa_a^b$  will be constrained to be  $[0.40, 0.78]$  and  $[0.0, 1.2]$  at the  $1\sigma$  level when we consider  $\kappa_a^b$  alone in the analysis with  $\mu_{Zh}^0 = 0.93$  and  $\mu_{Zh}^0 = 1$ , respectively. Moreover, the other anomalous couplings will not change the conclusion noticeably, cf. Figs. 3 and 4. We also note that the uncertainties of  $\kappa_a^b$ , with our benchmark  $\mu_{Zh}^0$  value, at the HL-LHC are larger than that constrained by the current LHC data, cf. Fig. 2(a). It arises from the fact that the  $1\sigma$  upper limit of the signal strength in the large transverse momentum region of  $pp \rightarrow Zh$  production, at the 13 TeV LHC, just reaches the SM prediction.

**Break the  $Z\bar{b}b$  coupling degeneracy:** The  $Zb\bar{b}$  couplings are also well constrained by the LEP and SLC electroweak data and mainly determined by the  $Z$ -pole measurements at the LEP:  $R_b$  and  $A_{FB}^b$ . The  $R_b$  is defined by the following ratio,

$$R_b = \frac{\Gamma(Z \rightarrow b\bar{b})}{\sum_q \Gamma(Z \rightarrow q\bar{q})}, \quad (6)$$

where the sum in the denominator includes all quarks except the top quark. The  $R_b$  measurement agrees with the SM prediction very well, while the  $A_{FB}^b$  at the  $Z$ -pole exhibits a large deviation from the SM prediction with a significance around  $2.5\sigma$  [1, 47]. The SLC with polarized beam can directly probe the bottom quark asymmetry  $A_b$  which was found to be consistent with the SM within  $1\sigma$  [1]. As pointed out in Ref. [2], the  $Z$ -pole data alone can not fully determine the  $Zb\bar{b}$  interactions due to the sign ambiguities of the couplings. With the help of  $A_{FB}^b$  measurements conducted in the off-shell  $Z$  boson region, the part of parameter space with  $\kappa_{a,v}^b < 0$  has been excluded. However, it remains to be difficult to resolve the apparent degeneracy in the parameter space with  $\kappa_{a,v}^b > 0$  due to the limited statistics for data away from the  $Z$ -pole. As shown in Fig. 5, both sets of  $\kappa_a^b$  and

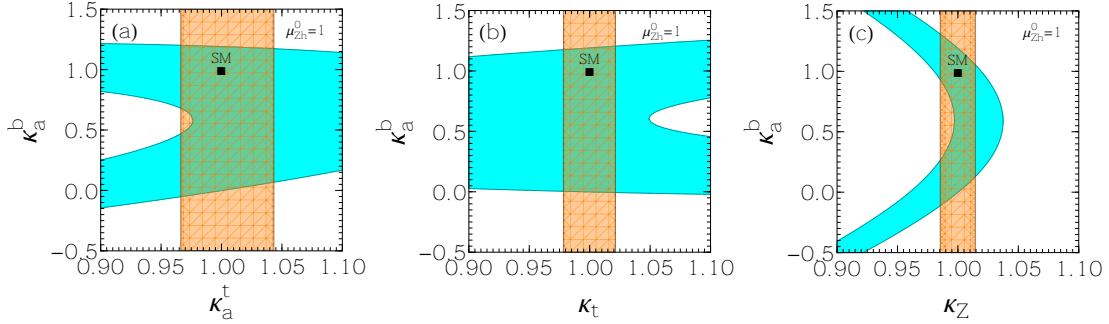


FIG. 4. Similar to Fig. 3, but for  $\mu_{Zh}^0 = 1$ .

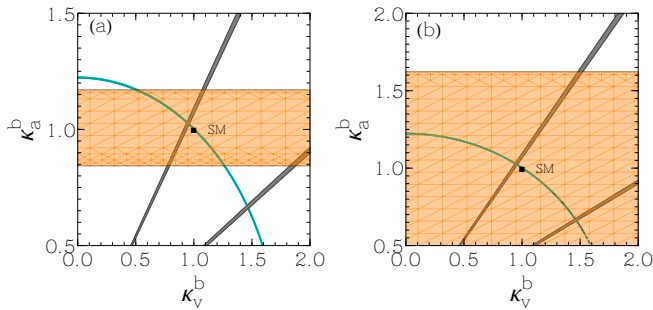


FIG. 5. Present constraints on the axial-vector  $Zb\bar{b}$  coupling  $\kappa_a^b$ . The cyan and gray regions come from the  $R_b$ ,  $A_{FB}^b$ , and  $A_b$  measurements at LEP and SLC, respectively. The orange band in (a) comes from the measurements of inclusive cross section and  $p_T^Z$  distribution of  $Zh$  associated production at the 13 TeV LHC, while (b) is the result after removing the two high  $p_T^Z$  data in Fig. 4 of Ref. [32].

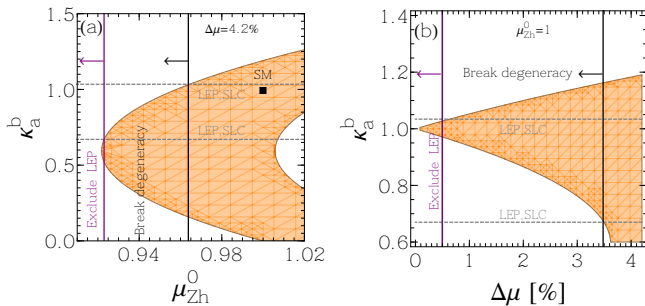


FIG. 6. Expected signal strength  $\mu_{Zh}^0$  (a) and precision  $\Delta\mu$  (b) for breaking the  $Zb\bar{b}$  coupling degeneracy (black perpendicular line) and excluding LEP  $A_{FB}^b$  measurement (purple perpendicular line) at the 14 TeV LHC. The two gray (horizontal) dashed lines indicate the degeneracy (at  $\kappa_a^b = 1.03$  and  $0.67$ ) found in the analysis of LEP and SLC data. The orange band in (a) shows the expected uncertainty on the determination of  $\kappa_a^b$  from measuring the inclusive cross section of the  $Zh$  production at the HL-LHC with a fixed  $\Delta\mu = 4.2\%$ , while (b) is the similar result but with a fixed  $\mu_{Zh}^0 = 1$ .

$\kappa_v^b$  values, with  $(\kappa_a^b, \kappa_v^b) = (1.03, 0.95)$  or  $(0.67, 1.46)$ , are consistent with the precision electroweak data at LEP and SLC.

To break this degeneracy, one needs to analyze the  $Zh$  data collected at LHC. In Fig. 5, we compare the precision on the determination of the axial-vector component of the  $Zb\bar{b}$  anomalous coupling via the measurements of inclusive cross section and transverse momentum distribution of  $Z$  boson in the  $Zh$  production at the 13 TeV LHC to that implied by the precision electroweak data at LEP and SLC. Here, we focus on the parameter space with  $\kappa_{a,v}^b > 0$ . The cyan and gray shaded regions denote the constraint from  $R_b$  and  $(A_{FB}^b, A_b)$  measurements with  $1\sigma$  accuracy, respectively. The orange region in Fig. 5(a) is consistent with the current  $Zh$  production measurements, while the orange band in Fig. 5(b) shows the allowed parameter space region after we remove the above-mentioned two high  $p_T^Z$  data points [32]. It is evident that the current measurement of the  $Zh$  inclusive cross section at the LHC has broken the degeneracy in the allowed  $\kappa_a^b$  and  $\kappa_v^b$  values implied by the precision electroweak data, resulting the preferred values of  $\kappa_a^b$  and  $\kappa_v^b$  to be close to 1, the SM values. However, the degeneracy would remain after removing the two high  $p_T^Z$  data points whose central values are smaller than the SM predictions. Hence, it is important to have a more precise measurement of the  $p_T^Z$  distribution in the  $Zh$  events at the LHC.

It appears that the precision electroweak measurements at the LEP and SLC, as compared to the measurements of  $Zh$  inclusive cross section at the LHC, yield the strongest constraint on  $\kappa_a^b$ , cf. Fig. 5. However, this conclusion depends on the value of  $\mu_{Zh}^0$  which needs to be better measured at the HL-LHC. The expected constraint on  $\kappa_a^b$  derived from the  $Zh$  inclusive cross section measurement at the HL-LHC, assuming an projected uncertainty  $\Delta\mu = 4.2\%$  [46], is shown as the orange band in Fig. 6(a), in which the two horizontal lines indicate the two values (1.03 and 0.67) of  $\kappa_a^b$  consistent with the precision electroweak data at LEP and SLC. The degeneracy of  $\kappa_a^b$  (and  $\kappa_v^b$ ) found in interpreting the precision

electroweak data at LEP and SLC can be broken by the measurement of  $Zh$  production cross section at HL-LHC if  $\mu_{Zh}^0$  is measured to be less than 0.964 (indicated by the black perpendicular line), which excludes the solution of  $\kappa_a^b = 1.03$  allowed by the precision electroweak data and implies new physics beyond the SM must exist (for  $\mu_{Zh}^0 \neq 1$ ). In case that  $\mu_{Zh}^0$  is measured to be less than 0.923 (indicated by the purple perpendicular line), the  $Zh$  cross section measurement at HL-LHC would exclude the interpretation of the precision electroweak data at LEP and SLC by introducing merely the anomalous  $\kappa_a^b$  and  $\kappa_v^b$  couplings. Moreover, in that case,  $\kappa_a^b$  can be well determined.

On the other hand, when  $\mu_{Zh}^0 = 1$ , it becomes challenging to test against the  $A_{FB}^b$  measurement at LEP by measuring the  $Zh$  cross section at HL-LHC, due to the large uncertainty in  $\kappa_a^b$ , cf. Fig. 4. To achieve that goal, a much higher precision of the  $Zh$  cross section measurement is needed. Fig. 6(b) shows the required precision  $\Delta\mu$  to break the apparent degeneracy in the  $Z\bar{b}b$  couplings, as implied by the LEP and SLC electroweak data, is 3.5% (black perpendicular line). To exclude the interpretation of the  $A_{FB}^b$  data at LEP by introducing merely the anomalous  $\kappa_a^b$  and  $\kappa_v^b$  couplings would require  $\Delta\mu = 0.5\%$  (indicated by the purple perpendicular line). However, current study on the  $Zh$  cross section measurement at HL-LHC [46] projects a 2.6% statistical error, 1.3% experimental systematic error and 3.1% theoretical uncertainty. Hence,  $\Delta\mu = 3.5\%$  might be hopeful to reach at HL-LHC, with an improvement in the theoretical calculation accuracy. But, it would be very challenging to reach  $\Delta\mu = 0.5\%$ . Nevertheless, measuring the cross section of  $Zh$  production can clearly break the apparent degeneracy of the  $Z\bar{b}b$  couplings, as implied by the precision electroweak data at LEP and SLC.

**Conclusions:** In this Letter, we propose a novel signature to probe the anomalous  $Z\bar{b}b$  couplings through measuring the cross section of the  $Zh$  associated production via gluon-gluon fusion at the LHC. Our method could be used to break the apparent degeneracy in the  $Z\bar{b}b$  couplings, as implied by the LEP and SLC precision electroweak data, including the long-standing discrepancy of the  $A_{FB}^b$  data from LEP. We show that the  $Zh$  cross section at the one-loop level only depends on the axial-vector component of the  $Z\bar{b}b$  coupling. The precision on the measurement of  $\kappa_a^b$  is sensitive to the central value of the signal strength ( $\mu_{Zh}^0$ ) of  $Zh$  production, and the limit on  $\kappa_a^b$  is not sensitive to the other anomalous couplings, e.g.  $Zt\bar{t}$ ,  $ht\bar{t}$  and  $hZZ$  couplings. If  $\mu_{Zh}^0$  is found to be noticeably less than 1, the degeneracy of the  $Z\bar{b}b$  couplings found interpreting the precision electroweak data at LEP and SLC can be broken and new physics beyond the SM must exist.

**Acknowledgements.** This work is partially supported

by the U.S. Department of Energy, Office of Science, Office of Nuclear Physics, under Contract DE-AC52-06NA25396, [under an Early Career Research Award (C. Lee),] and through the LANL/LDRD Program, as well as the U.S. National Science Foundation under Grant No. PHY-2013791. C.-P. Yuan is also grateful for the support from the Wu-Ki Tung endowed chair in particle physics.

---

\* [binyan@lanl.gov](mailto:binyan@lanl.gov)

† [yuan@pa.msu.edu](mailto:yuan@pa.msu.edu)

- [1] S. Schael et al. (ALEPH, DELPHI, L3, OPAL, SLD, LEP Electroweak Working Group, SLD Electroweak Group, SLD Heavy Flavour Group), Phys. Rept. **427**, 257 (2006), hep-ex/0509008.
- [2] D. Choudhury, T. M. Tait, and C. Wagner, Phys. Rev. D **65**, 053002 (2002), hep-ph/0109097.
- [3] K. Agashe, R. Contino, L. Da Rold, and A. Pomarol, Phys. Lett. B **641**, 62 (2006), hep-ph/0605341.
- [4] D. Liu, J. Liu, C. E. M. Wagner, and X.-P. Wang, Phys. Rev. D **97**, 055021 (2018), 1712.05802.
- [5] M. Bicer et al. (TLEP Design Study Working Group), JHEP **01**, 164 (2014), 1308.6176.
- [6] (2013), 1306.6352.
- [7] S. Gori, J. Gu, and L.-T. Wang, JHEP **04**, 062 (2016), 1508.07010.
- [8] M. Dong et al. (CEPC Study Group) (2018), 1811.10545.
- [9] R. V. Harlander, S. Liebler, and T. Zirke, JHEP **02**, 023 (2014), 1307.8122.
- [10] B. Hespel, F. Maltoni, and E. Vryonidou, JHEP **06**, 065 (2015), 1503.01656.
- [11] C. Englert, M. McCullough, and M. Spannowsky, Phys. Rev. D **89**, 013013 (2014), 1310.4828.
- [12] L. M. Carpenter, T. Han, K. Hendricks, Z. Qian, and N. Zhou, Phys. Rev. D **95**, 053003 (2017), 1611.05463.
- [13] C. Englert, R. Rosenfeld, M. Spannowsky, and A. Tonero, EPL **114**, 31001 (2016), 1603.05304.
- [14] A. Azatov, C. Grojean, A. Paul, and E. Salvioni, JHEP **09**, 123 (2016), 1608.00977.
- [15] D. Goncalves and J. Nakamura, Phys. Rev. D **98**, 093005 (2018), 1805.06385.
- [16] R. Harlander, J. Klappert, C. Pandini, and A. Papaefstathiou, Eur. Phys. J. C **78**, 760 (2018), 1804.02299.
- [17] E. Vryonidou and C. Zhang, JHEP **08**, 036 (2018), 1804.09766.
- [18] C. Degrande, F. Maltoni, K. Mimasu, E. Vryonidou, and C. Zhang, JHEP **10**, 005 (2018), 1804.07773.
- [19] Q.-H. Cao and B. Yan, Phys. Rev. D **92**, 094018 (2015), 1507.06204.
- [20] Q.-H. Cao, S.-L. Chen, and Y. Liu, Phys. Rev. D **95**, 053004 (2017), 1602.01934.
- [21] O. Bessidskaia Bylund, F. Maltoni, I. Tsirikos, E. Vryonidou, and C. Zhang, JHEP **05**, 052 (2016), 1601.08193.
- [22] Q.-H. Cao, S.-L. Chen, Y. Liu, R. Zhang, and Y. Zhang, Phys. Rev. D **99**, 113003 (2019), 1901.04567.
- [23] G. Li, L.-X. Xu, B. Yan, and C.-P. Yuan, Phys. Lett. B **800**, 135070 (2020), 1904.12006.
- [24] Q.-H. Cao, B. Yan, C. Yuan, and Y. Zhang, Phys. Rev. D **102**, 055010 (2020), 2004.02031.

- [25] W. Buchmuller and D. Wyler, Nucl. Phys. B **268**, 621 (1986).
- [26] G. Giudice, C. Grojean, A. Pomarol, and R. Rattazzi, JHEP **06**, 045 (2007), hep-ph/0703164.
- [27] B. Grzadkowski, M. Iskrzynski, M. Misiak, and J. Rosiek, JHEP **10**, 085 (2010), 1008.4884.
- [28] T. Hahn, Comput. Phys. Commun. **140**, 418 (2001), hep-ph/0012260.
- [29] V. Shtabovenko, R. Mertig, and F. Orellana, Comput. Phys. Commun. **207**, 432 (2016), 1601.01167.
- [30] B. A. Kniehl and C. P. Palisoc, Phys. Rev. D **85**, 075027 (2012), 1112.1575.
- [31] J. Alwall, R. Frederix, S. Frixione, V. Hirschi, F. Maltoni, O. Mattelaer, H. S. Shao, T. Stelzer, P. Torrielli, and M. Zaro, JHEP **07**, 079 (2014), 1405.0301.
- [32] G. Aad et al. (ATLAS) (2020), 2008.02508.
- [33] M. Aaboud et al. (ATLAS), Phys. Lett. B **786**, 59 (2018), 1808.08238.
- [34] M. Aaboud et al. (ATLAS), JHEP **05**, 141 (2019), 1903.04618.
- [35] G. Aad et al. (ATLAS) (2020), 2007.02873.
- [36] CMS-PAS-HIG-19-005 (2020).
- [37] D. de Florian et al. (LHC Higgs Cross Section Working Group), **2/2017** (2016), 1610.07922.
- [38] A. Hasselhuhn, T. Luthe, and M. Steinhauser, JHEP **01**, 073 (2017), 1611.05881.
- [39] A. M. Sirunyan et al. (CMS), Phys. Rev. Lett. **122**, 132003 (2019), 1812.05900.
- [40] M. Aaboud et al. (ATLAS), Phys. Lett. B **784**, 173 (2018), 1806.00425.
- [41] A. M. Sirunyan et al. (CMS), Phys. Rev. Lett. **120**, 231801 (2018), 1804.02610.
- [42] A. M. Sirunyan et al. (CMS), JHEP **03**, 056 (2020), 1907.11270.
- [43] M. Aaboud et al. (ATLAS), Phys. Rev. D **99**, 072009 (2019), 1901.03584.
- [44] G. Aad et al. (ATLAS), JHEP **07**, 124 (2020), 2002.07546.
- [45] G. Aad et al. (ATLAS), Eur. Phys. J. C **80**, 957 (2020), 2004.03447.
- [46] M. Cepeda et al., CERN Yellow Rep. Monogr. **7**, 221 (2019), 1902.00134.
- [47] M. Baak, J. Cúth, J. Haller, A. Hoecker, R. Kogler, K. Mönig, M. Schott, and J. Stelzer (Gfitter Group), Eur. Phys. J. C **74**, 3046 (2014), 1407.3792.